**DOI:** 10.11858/gywlxb.20240719

# Pressure-Induced Polymerization of One-Dimensional Nitrogen Chains in $K_2N_2$

CHEN Lei[1], ZHANG Yun[1], CHEN Yuxuan[1], WEI Qun[2], ZHANG Meiguang[1]

（1. *College of Physics and Optoelectronic Technology*, *Baoji University of Arts and Sciences*, *Baoji* 721013, *Shaanxi*, *China* ;
2. *School of Physics*, *Xidian University*, *Xi'an* 710071, *Shaanxi*, *China*）

**Abstract:** The crystal structure prediction of $K_2N_2$ in the pressure range of 0–150 GPa using an advanced particle swarm crystal structure search method was conducted. The results show that the stable ground state phase of $K_2N_2$ is a monoclinic *C*2/*m* structure, and three high-pressure structures including $Na_2N_2$-type, *Cmmm*, and *C*2/*c* are identified at pressures of 1.7, 3.6, 122 GPa, respectively. The volume dependence on pressure shows that the three phase transitions, i. e., *C*2/*m*→$Na_2N_2$-type, $Na_2N_2$-type→*Cmmm*, and *Cmmm*→*C*2/*c*, are all first order phase transitions, corresponding to volume collapses of 14.4%, 22.5%, and 4.0%, respectively. During the high pressure phase transitions of $K_2N_2$, the coordination number of K atom increases from 5 to 10, and a change in the nature of the N-N bonding from N＝N dimmer in the ground state of *C*2/*m* structure to N－N single bond chain in the high-pressure *C*2/*c* phase is accompanied. The high-pressure *C*2/*c* phase exhibits semiconducting properties with a band gap of 2.0 eV, while *C*2/*m*, $Na_2N_2$-type, and *Cmmm* phases have metallic behaviors. Electronic structure calculation and electron-localized function analysis indicate that the high-pressure structural phase transition of $K_2N_2$ is due to the K-*p* lone-pair electrons activation and their participation in bonding with N atoms under high pressure.

**Keywords:** high pressure; $K_2N_2$; structure predictions; phase transitions; electronic structures

**CLC number:** O521.2 **Document code:** A

Metal nitrides have attracted increasing attention in a wide range application due to their fascinating properties, such as hardness, superconductivity, various types of magnetism, etc.[1−2] Recently, extensive efforts have focused on the synthesis and design of metal polynitrides with single and double nitrogen bonds under high pressure, as metal polynitrides are proposed to be promissing candidates for high-energy density materials (HEDMs)[3−5]. The decomposition of these polynitrides is expected to release huge energy due to the conversion from a single/double-bonded polymeric nitrogen (160/418 kJ/mol) into a triple-bonded nitrogen (954 kJ/mol) molecule without producing pollutants. The atomic polymeric nitrogen with cubic gauche structure (cg-N) at a high pressure and high temperature (HPHT) condition (pressure above 110 GPa and temperature greater than 2 000 K) was successfully synthetized by Eremets *et al*.[6−8]. Motivated by that synthesis, alkali metal azides $AN_3$, constructed by spherical cations and linear molecular $N_3^-$ anions with N＝N double bonds, was proposed to be suitable precursor in the formation of polymeric nitrogen under pressure[9]. Experimentally, the polymeric

* **Received date:** 2024-01-29； **Revised date:** 2024-03-04

**Foundation item:** National Natural Science Foundation of China (11964026); Natural Science Basic Research Program of Shaanxi (2023-JC-YB-021, 2024JC-YBMS-048)

**Biography:** CHEN Lei (1983－), male, doctor, associate professor, major in high pressure materials and structures. E-mail: stonley@163.com

**Corresponding author:** ZHANG Meiguang (1981－), male, doctor, professor, major in high pressure materials and structures. E-mail: zhmgbj@126.com

evolutionary behaviors of $N_3^-$ anions in $LiN_3$[10], $NaN_3$[11–13], $KN_3$[14–16], $RbN_3$[17–18], and $CsN_3$[19–20] have been fully investigated under high pressure. One of the most interesting findings is the reported polymeric nitrogen nets in $NaN_3$[11] at 160 GPa. More recently, a fully $sp^2$-hybridized layered polymeric nitrogen structure, featuring fused 18-membered rings, in potassium supernitride ($K_2N_{16}$) was successfully synthesized under HPHT condition using a laser heating diamond anvil cell (DAC) technique[21]. In our previous works[22–25], the $N_3^-$ anions in $LiN_3$, $NaN_3$, and $KN_3$ all transform firstly to "$N_6$" molecular clusters under compression, and then to a polymerized nitrogen phase at high pressures.

Besides the well-known alkali metal azides $AN_3$, alkali metal diazenides $A_2N_2$ containing the N＝N double bonds, were also proposed as precursors of the polymeric atomic nitrogen under pressure. In 2010, two alkali metal diazenides, $Li_2N_2$ and $Na_2N_2$, were proposed to have orthorhombic *Pmmm* structure[26]. However, an orthorhombic *Immm* structure of $Li_2N_2$[27] was then synthesized under HPHT condition. Immediately after that, a serial pressure-induced structural phase transitions of $Li_2N_2$ were reported in two independent works[28–29]. Moreover, a high-pressure tetragonal $I4_1/acd$ phase containing the spiral nitrogen chain was uncovered at 242 GPa[29], indicating that the polymerization of nitrogen is realized from $Li_2N_2$.

Compared to $Li_2N_2$ and $Na_2N_2$, $K_2N_2$ have not been reported so far, neither for ambient pressure nor for high pressure. Here, we will extensively explore the high-pressure structures of $K_2N_2$ up to 150 GPa by using the first principles swarm structure searching method. The structure evolutions and chemical bonding behaviors of $K_2N_2$ within different structures were then fully studied to provide an insight into the formation of polymeric nitrogen in alkali metal diazenides.

## 1 Computational Method

The variable-cell crystal structure predictions for $K_2N_2$ (1–4 formula unit (f. u.) in the simulation cell) up to 150 GPa were conducted by CALYPSO code[30–31]. The effectiveness of this method has been fully confirmed in predicting high-pressure structures of various systems[32–35]. During the structure search process, the 60% structures of each generation with lower enthalpies were selected to generate the structures for the next generation by particle swarm optimization (PSO) technique, and the other structures in new generation were randomly generated to increase the structural diversity. Usually, the structure searching simulation stopped at the 20th generation and 40 structures per generation were generated at each pressure point. After finishing the structure search, the most stable structures were used for further structural relaxation and property calculation, a process that is implemented in the Vienna *ab Initio* Simulation Package[36]. The Perdew-Burke-Ernzerhof (PBE) exchange-correlation functional under the generalized gradient approximation[37] and the projector-augmented wave (PAW)[38] for ion-electron potentials were adopted herein. The van-der-Waals (vdW) correction was applied in the structural relaxation using Grimme's method (DFT-D3)[39]. The cutoff energy of 550 eV and Monkhorst-Pack *k* meshes[40] of $2\pi\times0.032$ Å$^{-1}$ were used to ensure the good convergences of total energy and maximum force on each atom. The lattice dynamic stability of each structure was checked by phonon spectrum obtained by PHONOPY code[41]. The charge transfer behavior of $K_2N_2$ was performed using Bader atoms-in-molecules (AIM) method[42].

## 2 Results and Discussion

### 2.1 Ground-State and High-Pressure Structures of $K_2N_2$

The ground-state structure for $K_2N_2$ at ambient pressure in our fully structural search (in Fig. 1(a)) is a monoclinic structure with the space group $C2/m$, which is different from those reported for $Li_2N_2$ and $Na_2N_2$[26]. In Fig. 1(a), the $N_2$ quasimolecule dimers in $C2/m$ structure are parallel to each other, and are tilted by a certain angle within *a*-*b* plane. The N-N bond length is 1.192 Å, which is a typical value for double bond. Also, the calculated

Mayer bond order[43] for the $N_2$ anion in the *C*2/*m* is 2.18, being consistent with double bond. Due to the weak interaction between the $N_2$ quasimolecules in the *C*2/*m* phase, the application of gigapascal pressure leads to the orientation change of $N_2$ quasimolecules and the structure transformation. Indeed, two stable orthorhombic structures, i.e. *Pmmm* and *Cmmm*, for $K_2N_2$ were uncovered at 2 and 5 GPa, respectively, as shown in Fig. 1(b) and Fig. 1(c). Remarkably, the unveiled *Pmmm* phase and the previously reported ground-state structure of $Na_2N_2$ are exactly isostructrual (the *Pmmm* phase denoted as the $Na_2N_2$-type phase hereafter), and the *Cmmm* phase of $K_2N_2$ and the high-pressure metastable structures of $Na_2N_2$ are isostructrual as well[26]. Furthermore, both $Na_2N_2$-type and *Cmmm* orthorhombic phases have the similar atomic arrangement that the parallel $N_2$ dimers are perpendicular to the K atomic layer. In the $Na_2N_2$-type and *Cmmm* phases, the calculated N-N bond lengths are 1.220 and 1.254 Å, while the characteristics of the N＝N double bond are as that of the *C*2/*m* structure in the ground-state. As the pressures rises to 150 GPa, a stable monoclinic *C*2/*c* structure, containing a folded one-dimensional nitrogen chains (see Fig. 1(d)), is identified for $K_2N_2$ for the first time. The lengths of two nonequivalent N-N bond in *C*2/*c* structure are 1.474 and 1.373 Å at 135 GPa, indicating genuine N－N single bond, and thus the nature of the structure is similar to that of the high-pressure phase of $NaN_3$[24]. Table 1 lists the structural details of the lattice parameters and the atomic positions of various $K_2N_2$ structures at selected pressure points.

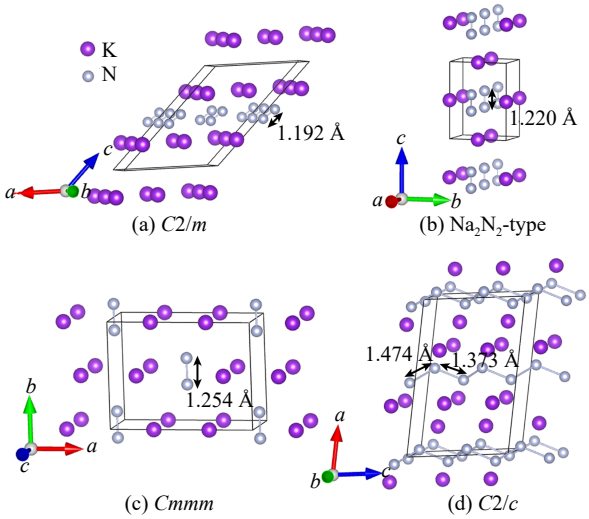



Fig. 1　Crystal structure of *C*2/*m*, $Na_2N_2$-type, *Cmmm*, and *C*2/*c* phases (The large and small spheres represent K and N atoms, respectively.)

**Table 1　Optimized structural parameters of the *C*2/*m*, $Na_2N_2$-type, *Cmmm*, and *C*2/*c* phases of $K_2N_2$**

| Phase | Pressure/GPa | Lattice parameters | $d_{N\text{-}N}$/Å | Atomic fractional coordinates |
|---|---|---|---|---|
| *C*2/*m* | 0 | $a$ = 7.562 Å, $b$ = 3.912 Å, $c$ = 10.923 Å, $\alpha = \gamma = 90°$, $\beta$= 134.955° | 1.192 | K 4i (0.613, 0, 0.260)<br>N 4i (0.519, 0, 0.456) |
| $Na_2N_2$-type | 2.5 | $a$ = 3.326 Å, $b$ = 4.375 Å, $c$ = 5.694 Å, $\alpha = \beta = \gamma = 90°$ | 1.220 | K1 1e (0, 0.500, 0)<br>K2 1c (0, 0, 0.500)<br>N 2t (0.500, 0.500, 0.393) |
| *Cmmm* | 20.0 | $a$ = 6.896 Å, $b$ = 5.104 Å, $c$ = 2.855 Å, $\alpha = \beta = \gamma = 90°$ | 1.254 | K 4g (0.694, 0, 0)<br>N 4j (0, 0.877, 0.500) |
| *C*2/*c* | 135.0 | $a$ = 6.971 Å, $b$ = 4.099 Å, $c$ = 4.510 Å, $\alpha = \gamma = 90°$, $\beta$= 81.342° | 1.474, 1.373 | K 8f (0.669, 0.909, 0.198)<br>N 8f (0.041, 0.887, 0.102) |

The phonon dispersion curves of the four predicted structures are illustrated in Fig. 2 in order to check their dynamic stabilities. Fig. 2 shows that all the $K_2N_2$ phases are dynamically stable as the eigen frequencies of their lattice vibrations are positive for all wavevectors in the Brillouin zone. It should be noted that the predicted *C*2/*m*, $Na_2N_2$-type, and *Cmmm* phases exhibit higher eigen frequencies of around 50 THz, which correspond to the vibrations of $N_2$ quasimolecules with stronger N＝N double bonds. By contrast, the *C*2/*c* phase shows relative lower vibration frequencies of around 30−35 THz, corresponding to the vibration frequencies of weaker N－N single bonds.

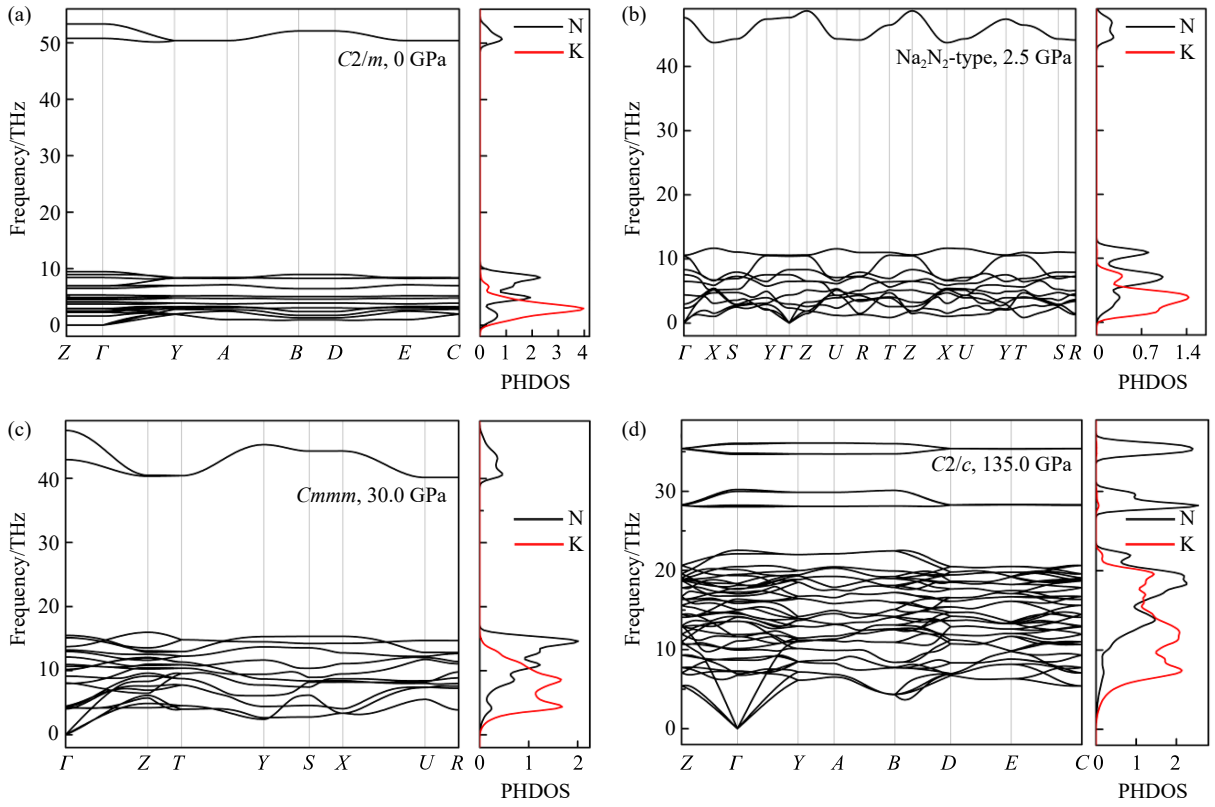



Fig. 2　Calculated phonon curves of the *C*2/*m* (a), $Na_2N_2$-type (b), *Cmmm* (c), and *C*2/*c* (d) phases at selected pressure points

Herein, we evaluated the energy involved in the decomposition of the *C*2/*c* phase with polymerized N—N single bond chains into metal K and gaseous $N_2$. The energy involved in the *C*2/*c*-$K_2N_2$ decompostion was determined to be 0.344 kJ/g, which is about three times of that of conventional energetic materials (0.104−0.105 kJ/g)[44], but much smaller than those reported for high-energy density materials (3.61 kJ/g for $BeN_4$, 5.30 kJ/g for $GaN_5$, 4.81 kJ/g for $GaN_{10}$)[45−46]. This may be due to the low nitrogen content in $K_2N_2$, so the nitrogen-rich $KN_x$ ($x$> 1) is expected to be potential HEDM under high pressure.

## 2.2　Pressure-Induced Structural Phase Transitions of $K_2N_2$

To determine the phase transition pressure of $K_2N_2$, we plotted in Figs. 3(a) and 3(b) the enthalpy difference of the predicted *C*2/*m*, *Cmmm*, and *C*2/*c* structures relative to the $Na_2N_2$-type phase in the pressure range of 0−150 GPa. The inset of Fig. 3(a) shows that above 1.7 GPa the $Na_2N_2$-type phase becomes energetically preferable with respect to the ground-state *C*2/*m* structure and is enthalpically stable up to about 3.6 GPa, above which it transforms into the *Cmmm* structure. From Fig. 3(b), it can be seen that the *Cmmm* structure persists up to 122 GPa and then transforms to the *C*2/*c* structure according to our structural predictions and enthalpy difference calculations. The wide pressure range of stable *Cmmm* phase may be attributed to the relative smaller ionic radius and atomic mass of K atom, in contrast with the heavier Rb and Cs atoms. It is thus expected that the chemical precompression exerted by heavier atoms, such as Rb and Cs, in $A_2N_2$ (as for $Cs_2N_2$[43]) can yield lower pressures for the polymerization of one-dimension N chains. From the calculated pressure dependence of the volume per f. u. in Figs. 3(c) and 3(d), the volume collapses of the first-order transformations *C*2/*m*→$Na_2N_2$-type, $Na_2N_2$-type→*Cmmm*, and *Cmmm*→*C*2/*c* are 14.4%, 22.5%, and 4.0% respectively. Thus, the *Cmmm* phase is much stiffer than low-pressure *C*2/*m* and $Na_2N_2$-type phases under compression. This is consistent with the increasing coordination number of the K atom in the different $K_2N_2$ phases under compression in Figs. 3(c) and 3(d). The densification of $K_2N_2$ under pressure is realized by increasing the cation coordination number from 5 in ground-

state *C*2/*m* phase to 8 in $Na_2N_2$-type (K2 atoms are coordinated by eight N atoms and K1 atoms are fourfold coordinated by four N atoms) and *Cmmm* phases, and finally to 10 in *C*2/*c* phase.

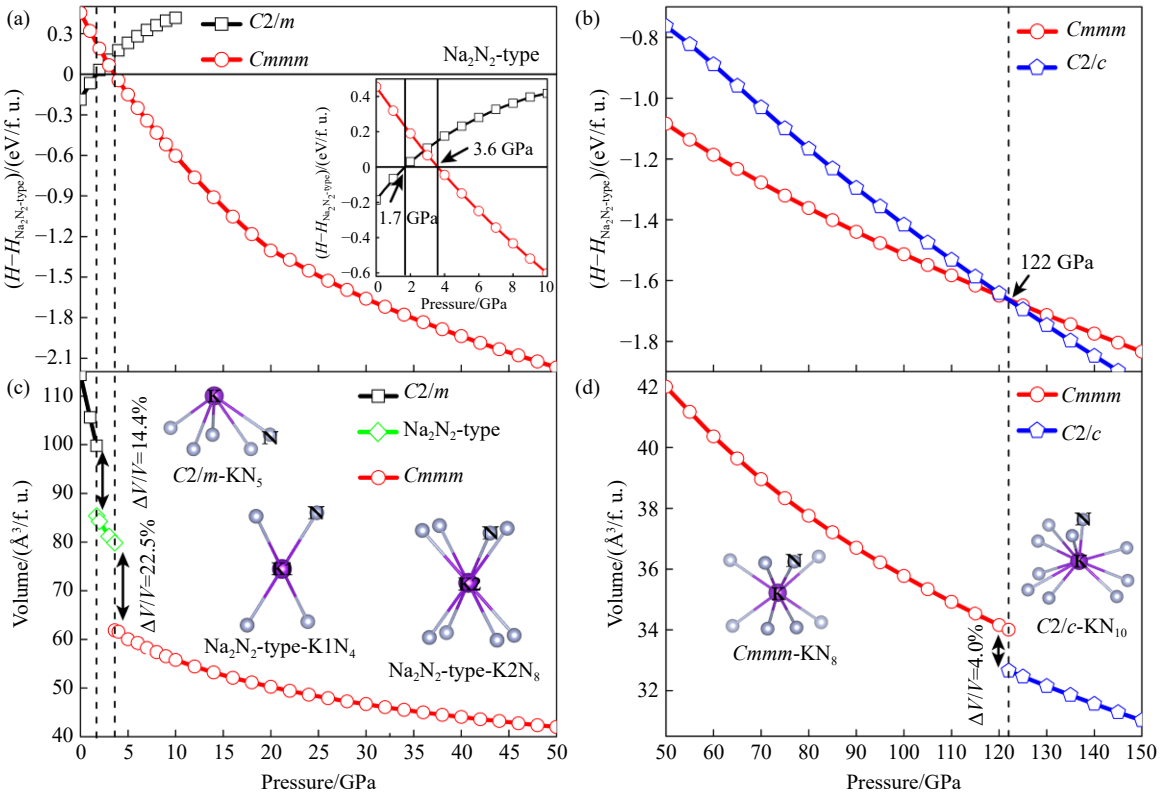



Fig. 3　(a)–(b) Enthalpy differences of the different predicted structures relative to the $Na_2N_2$-type structure under pressure; (c)–(d) pressure dependence of the volume per f. u. of each structure for $K_2N_2$

## 2.3　Electronic Structures of $K_2N_2$ Phases

To get deeper insight into the electronic structure evolutions of these $K_2N_2$ phases under pressure, we calculated the total density of states (DOS) and the site projected DOS, as shown in Fig. 4, where the Fermi level is the vertical dotted line. In contrast with the semiconducting nature of *C*2/*c* phase (Fig. 4(d)), the *C*2/*m*, $Na_2N_2$-type, and *Cmmm* phases are all metallic with the N-*p* electron crossing the Fermi level. Thus, the $K_2N_2$ possesses a metal-semiconductor transition, that is similar to that of Li-N system in recent work[28]. From Fig. 4(a)–Fig. 4(c), the *C*2/*m*, $Na_2N_2$-type, and *Cmmm* phases exhibit similar projected DOS profiles in the valence band region, the K-*s* and K-*p* atomic orbitals are located at the deep energy levels (around −32 and −16 eV, respectively), and the N-*s* atomic orbitals mainly lie around −22 − −10 eV. Moreover, the interaction between K and N atoms is extremely weak due to the absence of overlapping regions in their atomic projected DOSs. From the inspection of the DOS profiles, a clear broadening of different atomic decomposed states is seen in the high-pressure *C*2/*c* phase (Fig. 4(d)), leading to clear hybridizations between K-*p* and N-*p* atomic orbitals. In contrast to the first three low-pressure $K_2N_2$ phases, this distinction is partially due to the increasing coordination number of K atoms in *C*2/*c* phase and to the resulting chemical bonding change that will be illustrated in the following Bader charge transfer analysis.

Fig. 5 presents the PBE-resulted energy band structures of the four $K_2N_2$ phases, the projected weights of K-*s*, K-*p*, and N-*s* orbital electrons are not taken into account herein because of their exceptionally tiny contributions around the Fermi level in Fig. 4. Compared to the strong metallic nature of the *Cmmm* phase, which is mainly dominated by N-$p_x$/N-$p_z$ at the considered energy range of −2 − 2 eV (Fig. 5(c)), the *C*2/*m* ( $Na_2N_2$-type) phase

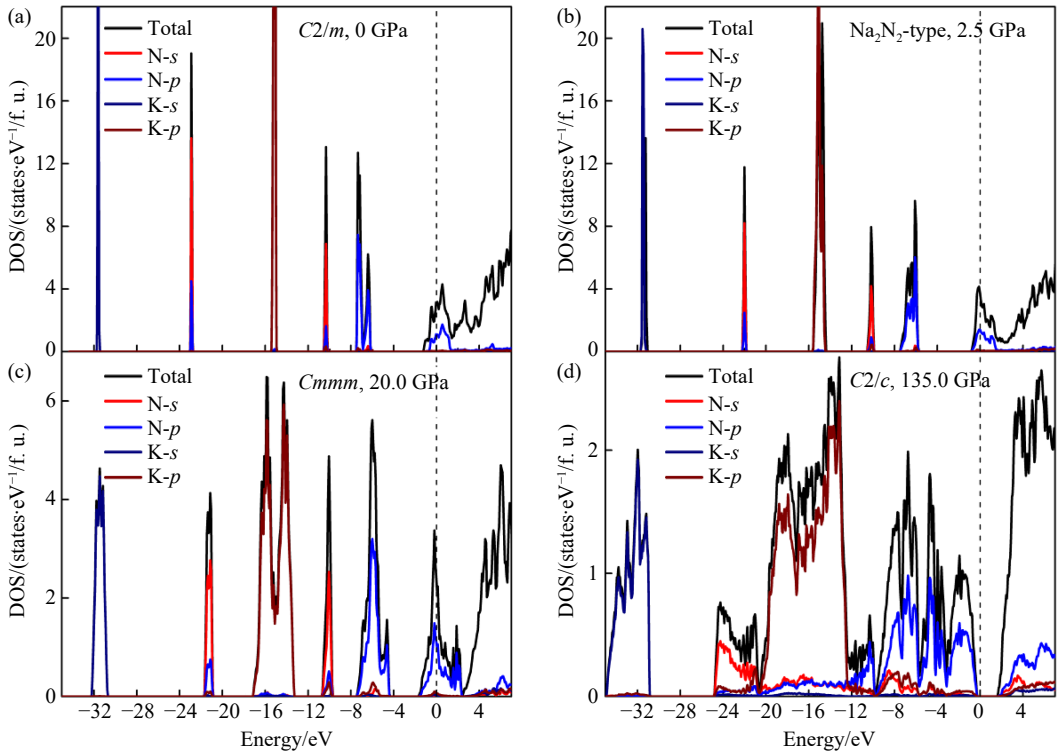
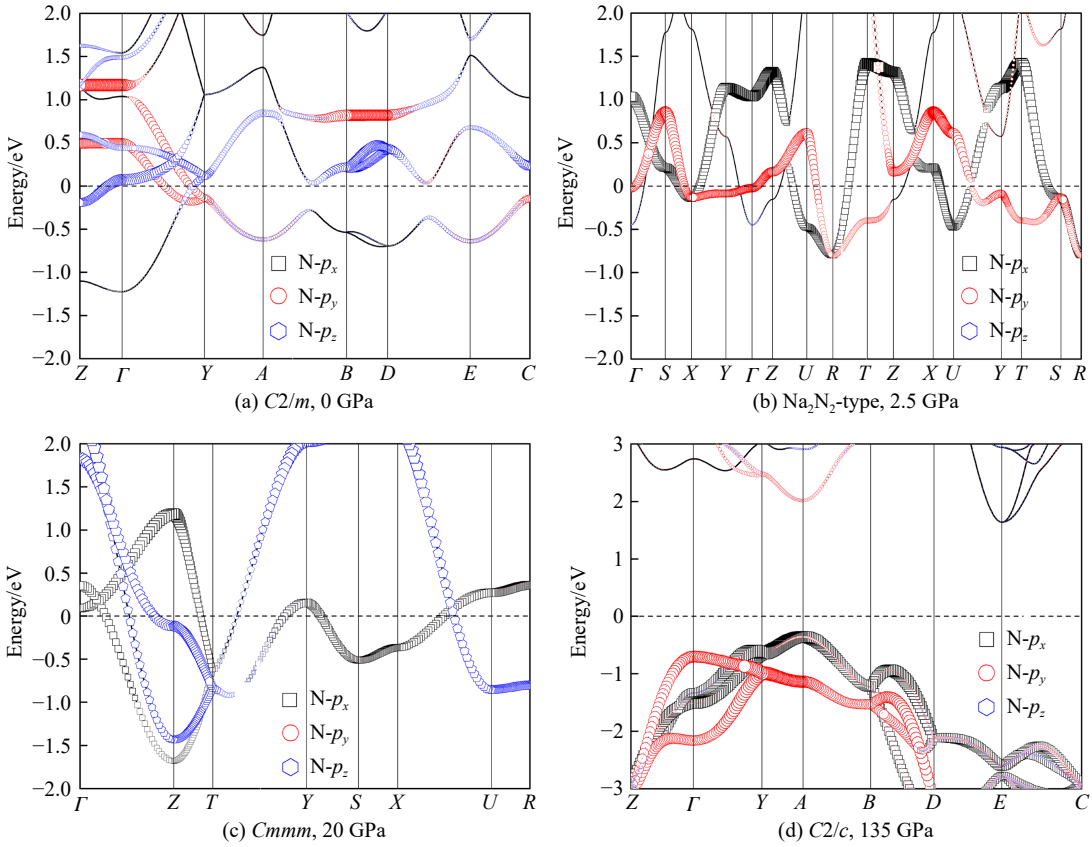



Fig. 4　Total and site projected DOSs of *C*2/*m* (a), $Na_2N_2$-type (b), *Cmmm* (c), and *C*2/*c* (d) phases




(a) *C*2/*m*, 0 GPa　(b) $Na_2N_2$-type, 2.5 GPa

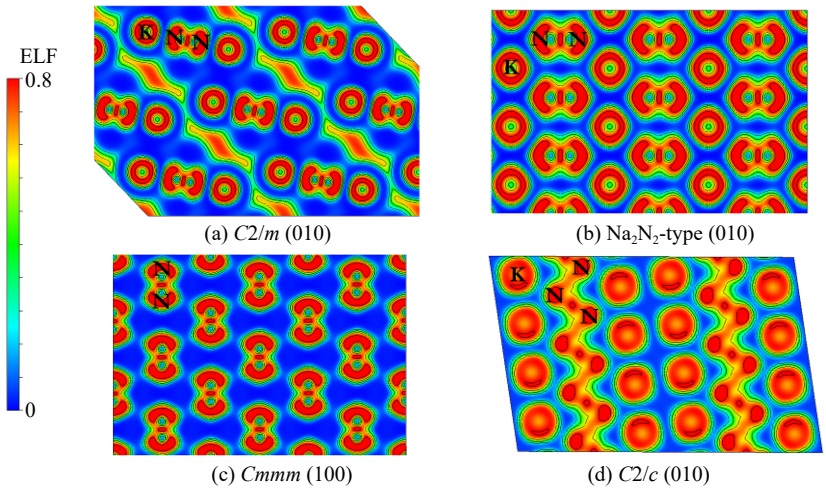
(c) *Cmmm*, 20 GPa　(d) *C*2/*c*, 135 GPa

Fig. 5　Projected weights of N-*p* orbitals in the band structures of *C*2/*m* (a), $Na_2N_2$-type (b), *Cmmm* (c), and *C*2/*c* phases (d) (The Fermi level is indicated by horizontal lines and the black solid lines denote the energy structures of each phase of $K_2N_2$)

exhibits a relative weaker metallic behavior that two bands of N-$p_y$/N-$p_z$ (N-$p_x$/N-$p_y$) crossing the Fermi level in Fig. 5(a) (Fig. 5(b)). The indirect semiconducting nature of *C*2/*c* phase (band gap of 2.0 eV) is demonstrated in Fig. 5(d), with the valence band maximum (VBM) and conduction band minimum (CBM) is located at *A* and *E* points, respectively. It is further found that the VBM and CBM of the *C*2/*c* phase are principally composed of N-$p_x$ and N-$p_z$ orbitals, respectively.

## 2.4　Atomic Chemical Bonding of $K_2N_2$ Phases

Fig. 6 shows the projected two-dimensional (2D) electron localization functions (ELF) of the four $K_2N_2$ phases to further reveal the atomic chemical bonding. The ELF is used to characterize the localized distribution of electrons of different atoms. The ELF values of 1, 0.5, and close to 0 indicate strong electron localization, electron gas, and nonelectron localization, respectively. From Fig. 6(a)–Fig. 6(c), the high-ELF regions are distributed between two N atoms, indicating the strong covalent N-N bonding in the *C*2/*m*, $Na_2N_2$-type, and *Cmmm* phases. Lone-pair electrons of K remain from the *C*2/*m* to *Cmmm* phases under pressure, as illustrated by the ELF value of 0 around K atoms, which is in conformity with the projected atomic orbital DOSs described in Fig. 4(a)–Fig. 4(c). For the compressed *C*2/*c* phase, some lone-pair electrons of K still remain, yet some of them are transferred to the regions of the K-N bond. Hence, the pressure compels the K-*p* lone-pair electrons to participate in the chemical bonding with N-*p* electrons under compression, realizing the high pressure *C*2/*c* phase with increased coordination number of K atoms. The electron localization on N-N bond in the *C*2/*c* phase (Fig. 6(d)) is weaker than that in the other three low-pressure $K_2N_2$ phases, confirming that the N—N single bond of the polymerized one-dimensional nitrogen chains is weaker than the N=N double bond of the $N_2$ quasimolecules.




(a) *C*2/*m* (010)　(b) $Na_2N_2$-type (010)

(c) *Cmmm* (100)　(d) *C*2/*c* (010)

Fig. 6　Contours of ELF for the *C*2/*m* on the (010) plane (a), $Na_2N_2$-type on the (010) plane (b), *Cmmm* on the (100) plane (c), and *C*2/*c* on the (010) plane (d)

Finally, the Bader charges in the four phases are listed in Table 2 by using the Bader AIM method. For the ground-state *C*2/*m* phase, each N atom accepts 0.491*e* which corresponds to the electron loss per K atom. When phase transits into the $Na_2N_2$-type and *Cmmm* phases, a relatively stronger ionic bonding feature of K-N bond is disclosed because that the charge transfer is raised to approximately 0.645*e* − 0.690*e* as a result of the electron gain of N. Contrarily, it is noted that the atomic charge transfer from the K atom to N atom decrease to 0.623*e* in the compressed *C*2/*c* phase. This variation may be originated from that partial K atoms participate in covalent bonding with the N atom under compression, as indicated by the orbital hybridizations of K-*p* and N-*p* in Fig. 4(d). It then can be concluded that the chemical bonding in the *C*2/*c* phase containing one-dimensional polymerized nitrogen chains is a complex mixture of covalent and ionic characteristics.

**Table 2　Calculated Bader charges of K and N atoms in *C*2/*m*, $Na_2N_2$-type, *Cmmm*, and *C*2/*c* phases**

| Phase | Pressure/GPa | Atom | Charge value/*e* | Charge transfer/*e* |
|---|---|---|---|---|
| *C*2/*m* | 0 | K | 8.509 (×2) | +0.491 |
| | | N | 5.491 (×2) | −0.491 |
| $Na_2N_2$-type | 2.5 | K1 | 8.407 | +0.593 |
| | | K2 | 8.303 | +0.697 |
| | | N | 5.645 (×2) | −0.645 |
| *Cmmm* | 20.0 | K | 8.310 (×2) | +0.690 |
| | | N | 5.690 (×2) | −0.690 |
| *C*2/*c* | 135.0 | K | 8.377 (×2) | +0.623 |
| | | N | 5.623 (×2) | −0.623 |

## 3 Conclusions

In summary, we have performed a systematic crystal structure search for alkali metal diazenide $K_2N_2$ under pressure using the advanced swarm intelligence structure simulations. The ground-state phase of $K_2N_2$ is determined to be a new monoclinic *C*2/*m* structure with $N_2$ quasimolecules, and three high-pressure structures of $K_2N_2$, including $Na_2N_2$-type (1.7−3.6 GPa), *Cmmm* (3.6−122.0 GPa), and *C*2/*c* (above 122.0 GPa), are identified. Remarkably, the pressure-induced polymerization of one-dimensional nitrogen chains in the high-pressure *C*2/*c* semiconducting phase is firstly reported, attributed to the participation of K-*p* lone-pair electrons in the chemical bonding under pressure. The occurrences of the high-pressure phases of $Na_2N_2$-type, *Cmmm*, and *C*2/*c* follow the increased coordination numbers (from 5 to 10) of K atoms with the incresed pressures, accompanied by significant N-N bonding modification from N＝N dimers to polymerized N－N single bond one-dimensional chains. Furthermore, a metal-semiconductor transition of $K_2N_2$ under pressure is demonstrated by the electronic structures calculations. The present findings provide fundamental insights into the high-pressure structures and the polymerization of N atoms of alkali metal diazenides, supplying useful guidance for the syntheses of $K_2N_2$ in further experimental efforts.

## References:


[1] PIERSON H O. Handbook of refractory carbides and nitrides: properties, characteristics, processing and applications [M]. Westwood: Noyes, 1996.

[2] HORVATH-BORDON E, RIEDEL R, ZERR A, et al. High-pressure chemistry of nitride-based materials [J]. Chemical Society Reviews, 2006, 35(10): 987–1014.

[3] CHRISTE K O. Polynitrogen chemistry enters the ring: a cyclo-$N_5^-$ anion has been synthesized as a stable salt and characterized [J]. Science, 2017, 355(6323): 351.

[4] LANIEL D, WECK G, LOUBEYRE P. Direct reaction of nitrogen and lithium up to 75 GPa: synthesis of the $Li_3N$, LiN, $LiN_2$, and $LiN_5$ compounds [J]. Inorganic Chemistry, 2018, 57(17): 10685–10693.

[5] YAO Y S, ADENIYI A O. Solid nitrogen and nitrogen-rich compounds as high-energy-density materials [J]. Physica Status Solidi (B), 2021, 258(6): 2000588.

[6] EREMETS M I, GAVRILIUK A G, TROJAN I A, et al. Single-bonded cubic form of nitrogen [J]. Nature Materials, 2004, 3(8): 558–563.

[7] EREMETS M I, GAVRILIUK A G, TROJAN I A. Single-crystalline polymeric nitrogen [J]. Applied Physics Letters, 2007, 90(17): 171904.

[8] GREGORYANZ E, GONCHAROV A F, SANLOUP C, et al. High *P*-*T* transformations of nitrogen to 170 GPa [J]. The Journal of Chemical Physics, 2007, 126(18): 184505.

[9] ZHANG L J, WANG Y C, LV J, et al. Materials discovery at high pressures [J]. Nature Reviews Materials, 2017, 2(4): 17005.

[10] MEDVEDEV S A, TROJAN I A, EREMETS M I, et al. Phase stability of lithium azide at pressures up to 60 GPa [J]. Journal of Physics: Condensed Matter, 2009, 21(19): 195404.

[11] EREMETS M I, POPOV M Y, TROJAN I A, et al. Polymerization of nitrogen in sodium azide [J]. The Journal of Chemical Physics, 2004, 120(22): 10618–10623.

[12] ZHU H Y, ZHANG F X, JI C, et al. Pressure-induced series of phase transitions in sodium azide [J]. Journal of Applied Physics, 2013, 113(3): 033511.

[13] ZHOU M, LIU S J, DU M R, et al. High-pressure-induced structural and chemical transformations in $NaN_3$ [J]. The Journal of Physical Chemistry C, 2020, 124(37): 19904–19910.

[14] JI C, ZHANG F X, HOU D B, et al. High pressure X-ray diffraction study of potassium azide [J]. Journal of Physics and Chemistry of Solids, 2011, 72(6): 736–739.

[15] JI C, ZHENG R, HOU D B, et al. Pressure-induced phase transition in potassium azide up to 55 GPa [J]. Journal of Applied Physics, 2012, 111(11): 112613.

[16] WANG Y, BYKOV M, CHEPKASOV I, et al. Stabilization of hexazine rings in potassium polynitride at high pressure [J]. Nature Chemistry, 2022, 14(7): 794–800.

[17] LI D M, WU X X, JIANG J R, et al. Pressure-induced phase transitions in rubidium azide: studied by *in-situ* X-ray diffraction [J]. Applied Physics Letters, 2014, 105(7): 071903.

[18] LI D M, LI F F, LI Y, et al. High-pressure studies of rubidium azide by Raman and infrared spectroscopies [J]. The Journal of Physical Chemistry C, 2015, 119(29): 16870–16878.

[19] HOU D B, ZHANG F X, JI C, et al. Series of phase transitions in cesium azide under high pressure studied by *in situ* X-ray diffraction [J]. Physical Review B, 2011, 84(6): 064127.

[20] LI D M, ZHU P F, JIANG J R, et al. High-pressure Raman and infrared spectroscopic studies of cesium azide [J]. The Journal of Physical Chemistry C, 2016, 120(47): 27013–27018.

[21] SUI M H, LIU S, WANG P, et al. High-pressure synthesis of fully $sp^2$-hybridized polymeric nitrogen layer in potassium supernitride [J]. Science Bulletin, 2023, 68(14): 1505–1513.

[22] ZHANG M G, YAN H Y, WEI Q, et al. Novel high-pressure phase with pseudo-benzene "$N_6$" molecule of $LiN_3$ [J]. Europhysics Letters, 2013, 101(2): 26004.

[23] WANG X L, LI J F, BOTANA J, et al. Polymerization of nitrogen in lithium azide [J]. The Journal of Chemical Physics, 2013, 139(16): 164710.

[24] ZHANG M G, YIN K T, ZHANG X X, et al. Structural and electronic properties of sodium azide at high pressure: a first principles study [J]. Solid State Communications, 2013, 161: 13–18.

[25] ZHANG M G, YAN H Y, WEI Q, et al. A new high-pressure polymeric nitrogen phase in potassium azide [J]. RSC Advances, 2015, 5(16): 11825–11830.

[26] ZHANG X W, ZUNGER A, TRIMARCHI G. Structure prediction and targeted synthesis: a new $Na_nN_2$ diazenide crystalline structure [J]. The Journal of Chemical Physics, 2010, 133(19): 194504.

[27] SCHNEIDER S B, FRANKOVSKY R, SCHNICK W. High-pressure synthesis and characterization of the alkali diazenide $Li_2N_2$ [J]. Angewandte Chemie International Edition, 2012, 51(8): 1873–1875.

[28] SHEN Y Q, OGANOV A R, QIAN G R, et al. Novel lithium-nitrogen compounds at ambient and high pressures [J]. Scientific Reports, 2015, 5: 14204.

[29] ZHANG J, WANG X L, YANG K S, et al. The polymerization of nitrogen in $Li_2N_2$ at high pressures [J]. Scientific Reports, 2018, 8(1): 13144.

[30] WANG Y C, LV J, ZHU L, et al. Crystal structure prediction via particle-swarm optimization [J]. Physical Review B, 2010, 82(9): 094116.

[31] WANG Y C, LV J, ZHU L, et al. CALYPSO: a method for crystal structure prediction [J]. Computer Physics Communications, 2012, 183(10): 2063–2070.

[32] LI Y W, FENG X L, LIU H Y, et al. Route to high energy density polymeric nitrogen t-N via He-N compounds [J]. Nature Communications, 2018, 9(1): 722.

[33] MA L, WANG K, XIE Y, et al. High-temperature superconducting phase in clathrate calcium hydride $CaH_6$ up to 215 K at a

pressure of 172 GPa [J]. Physical Review Letters, 2022, 128(16): 167001.
[34] DUAN Q Z, SHEN J Y, ZHONG X, et al. Structural phase transition and superconductivity of ytterbium under high pressure [J]. Physical Review B, 2022, 105(21): 214503.
[35] SUN W G, CHEN B L, LI X F, et al. Ternary Na-P-H superconductor under high pressure [J]. Physical Review B, 2023, 107(21): 214511.
[36] KRESSE G, FURTHMÜLLER J. Efficient iterative schemes for *ab initio* total-energy calculations using a plane-wave basis set [J]. Physical Review B, 1996, 54(16): 11169–11186.
[37] PERDEW J P, BURKE K, ERNZERHOF M. Generalized gradient approximation made simple [J]. Physical Review Letters, 1996, 77(18): 3865–3868.
[38] BLÖCHL P E. Projector augmented-wave method [J]. Physical Review B, 1994, 50(24): 17953–17979.
[39] GRIMME S, ANTONY J, EHRLICH S, et al. A consistent and accurate *ab initio* parametrization of density functional dispersion correction (DFT-D) for the 94 elements H-Pu [J]. The Journal of Chemical Physics, 2010, 132(15): 154104.
[40] MONKHORST H J, PACK J D. Special points for Brillouin-zone integrations [J]. Physical Review B, 1976, 13(12): 5188–5192.
[41] TOGO A, TANAKA I. First principles phonon calculations in materials science [J]. Scripta Materialia, 2015, 108: 1–5.
[42] GATTI C. Chemical bonding in crystals: new directions [J]. Zeitschrift für Kristallographie-Crystalline Materials, 2005, 220(5/6): 399–457.
[43] PENG F, HAN Y X, LIU H Y, et al. Exotic stable cesium polynitrides at high pressure [J]. Scientific reports, 2015, 5(1): 16902.
[44] BRILL T B, JAMES K J. Kinetics and mechanisms of thermal decomposition of nitroaromatic explosives [J]. Chemical Reviews, 1993, 93(8): 2667–2692.
[45] ZHANG S T, ZHAO Z Y, LIU L L, et al. Pressure-induced stable $BeN_4$ as a high-energy density material [J]. Journal of Power Sources, 2017, 365: 155–161.
[46] ZHAI H, XU R, DAI J H, et al. Stabilized nitrogen framework anions in the Ga-N system [J]. Journal of the American Chemical Society, 2022, 144(47): 21640–21647.

# $K_2N_2$ 中一维氮链的压力诱导聚合

陈　磊[1], 张　云[1], 陈雨轩[1], 魏　群[2], 张美光[1]
（1. 宝鸡文理学院物理与光电技术学院, 陕西 宝鸡　721016;
2. 西安电子科技大学物理学院, 陕西 西安　710071）

**摘要:** 采用先进的粒子群晶体结构搜索方法对$K_2N_2$在0～150 GPa压强范围内进行晶体结构预测，结果表明，$K_2N_2$的基态稳定相为单斜$C2/m$结构，且在1.7、3.6和122 GPa压强下的结构分别为$Na_2N_2$型、$Cmmm$、$C2/c$。体积随压强的变化关系显示$C2/m$→$Na_2N_2$型、$Na_2N_2$型→$Cmmm$和$Cmmm$→$C2/c$这3个相变均为一级相变，对应的体积坍塌分别为14.4%、22.5%和4.0%。在$K_2N_2$高压相变过程中，K原子的配位数从5增加到10，并伴随着N-N成键性质的变化，即从基态$C2/m$结构中的准分子N＝N双键聚合为高压$C2/c$相中的N－N单键链。$C2/m$、$Na_2N_2$型、$Cmmm$相表现出金属性，而高压$C2/c$相表现出半导体（带隙为2.0 eV）性质。电子结构计算和电子局域函数分析表明，$K_2N_2$的高压结构相变来源于高压下K-$p$孤对电子的激活及其与N原子的成键。

**关键词:** 高压; $K_2N_2$; 结构预测; 结构相变; 电子结构
**中图分类号:** O521.2　　**文献标志码:** A